ACS APPLIED MATERIALS & INTERFACES

Research Article

www.acsami.org

Nitrogen-Enriched Hierarchically Porous Carbons Prepared from Polybenzoxazine for High-Performance Supercapacitors

Liu Wan,[†,‡] Jianlong Wang,[†] Lijing Xie,[†] Yahui Sun,[†,‡] and Kaixi Li*,[†]

[†]Institute of Coal Chemistry, Chinese Academy of Sciences, Taiyuan 030001, P.R. China

[‡]Graduate University of Chinese Academy of Sciences, Beijing 100049, P.R. China

Supporting Information

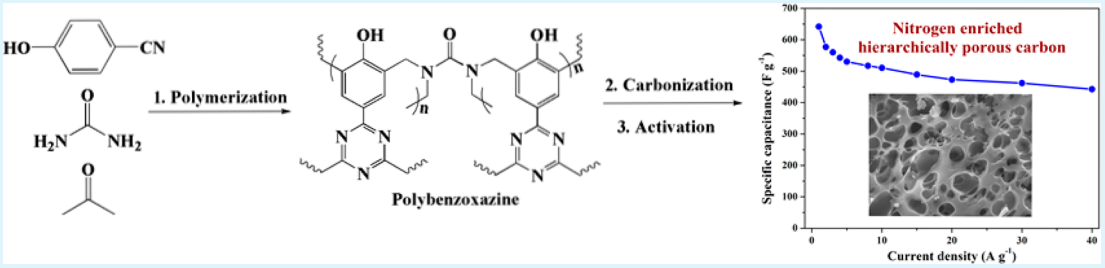

ABSTRACT: Nitrogen-enriched hierarchically porous carbons (HPCs) were synthesized from a novel nitrile-functionalized benzoxazine based on benzoxazine chemistry using a soft-templating method and a potassium hydroxide (KOH) chemical activation method and used as electrode materials for supercapacitors. The textural and chemical properties could be easily tuned by adding a soft template and changing the activation temperature. The introduction of the soft-templating agent (surfactant F127) resulted in the formation of mesopores, which facilitated fast ionic diffusion and reduced the internal resistance. The micropores of HPCs were extensively developed by KOH activation to provide large electrochemical double-layer capacitance. As the activation temperature increased from 600 to 800 °C, the specific surface area of nitrogen-enriched carbons increased dramatically, micropores were enlarged, and more meso/macropores were developed, but the nitrogen and oxygen content decreased, which affected the electrochemical performance. The sample HPC-800 activated at 800 °C possesses a high specific surface area (1555.4 $m^2 g^{-1}$), high oxygen (10.61 wt %) and nitrogen (3.64 wt %) contents, a hierarchical pore structure, a high graphitization degree, and good electrical conductivity. It shows great pseudocapacitance and the largest specific capacitance of 641.6 F g^{-1} at a current density of 1 A g^{-1} in a 6 mol L^{-1} KOH aqueous electrolyte when measured in a three-electrode system. Furthermore, the HPC-800 electrode exhibits excellent rate capability (443.0 F g^{-1} remained at 40 A g^{-1}) and good cycling stability (94.3% capacitance retention over 5000 cycles).

KEYWORDS: *supercapacitor, polybenzoxazine, hierarchically porous carbon, nitrogen functionalities*

1. INTRODUCTION

Supercapacitors, also called electrochemical capacitors, are becoming attractive power sources in memory backup devices, electric vehicles, military weapons, space equipment, and a number of day-today electric devices.[1,2] They combine the advantages of both dielectric capacitors and rechargeable batteries, which can deliver high power within a very small period and store high energy. On the basis of the charge-storage mechanism, supercapacitors can be divided into two categories: one is the electrical double-layer capacitor (EDLC), which stores energy by charge separation at the electrode/electrolyte interface; the other is the redox capacitor, which stores energy by the Faradaic reactions at the electrode/electrolyte surface.[3,4]

Carbon materials are regarded as the first candidate electrode materials for EDLCs. Recently, porous carbon materials, especially microporous activated carbons, have been widely adopted as the electrode materials for EDLCs because of their high surface area, excellent electric conductivity, high thermal and chemical stability, and low cost.[5,6] However, the intrinsically small micropores (<2 nm) of the activated carbons restrict quick electrolyte ion diffusion during the charge/discharge process. Thus, the surface of the micropores cannot be effectively utilized, which leads to low specific capacitances and poor rate capability.[7,8] In contrast, mesoporous or macroporous carbons can enable fast access of the electrolyte to the complete surface, especially under a high current condition. However, they exhibit also low capacitances and energy densities because of the less developed surface area and few micropores.[9] Hierarchically porous carbons (HPCs), especially possessing well-defined and interconnected micropores, mesopores, and macropores, are considered to be one of the promising electrode materials for supercapacitors, owing to the combined advantages of microporous carbons and meso/

Received: July 12, 2014
Accepted: August 19, 2014
Published: August 19, 2014

macroporuos carbons: high specific surface area, large pore volume, adjustable hierarchical pore structure, controlled surface chemistry, and good electric conductivity.[10−12]

The heteroatoms (such as nitrogen,[13] oxygen,[14] and phosphorus[15]) in a carbon network, which provide electron-donor characteristics to the carbon, can not only enhance the electronic conductivity and the wettability of the interface between the electrolyte and the electrode but also generate reversible pseudocapacitance. Therefore, nitrogen-enriched HPCs are proposed as ideal supercapacitor electrode materials with high capacitive performance. At present, various precursors have been applied to the preparation of nitrogen-doped porous carbons, such as polyacrylonitrile,[16] polyaniline,[17] and biomass or biomass derivatives.[18,19] Polybenzoxazine (PBZ), a new class of high-performance polymers, is considered to be one of the promising nitrogen-containing candidates because of its molecular design flexibility, excellent thermal properties, high char yield, nearly zero shrinkage, and the absence of volatiles during the curing process.[20−23] The thermoset PBZ resins can be easily prepared from inexpensive raw materials, including various phenols, primary amines, and formaldehyde.[24] Thus, the content and type of heteroatoms in PBZs can be easily changed by replacing the monofunctional amines or phenols by difunctional species, which is desirable for the controlled surface chemistry of HPCs.[25] However, few reports were focused on the synthesis of nitrogen-doped porous carbon materials based on PBZs.[26] Remarkably, high chemical and thermal stability of the PBZ make it possible to maintain high contents of nitrogen and oxygen species within the carbon matrix after carbonization and activation. It is beneficial for the synthesis of nitrogen-enriched porous carbons with high textural porosity and high char yield and the improvement of the wettability and conductivity of the obtained carbons. Therefore, PBZs are ideal precursors of the electrode materials for high-performance supercapactiors.

In this work, 4-cyanophenol as the phenol, diamine urea as the primary amine, and formaldehyde were selected to synthesize nitrile-functionalized benzoxazines via a solution method. The precursors, highly cross-linked PBZs, were obtained after the thermally activated ring-opening polymerization of the benzoxazines. The nitrogen-enriched HPCs were prepared from the PBZ by using a soft-templating method with potassium hydroxide chemical activation at different temperatures. The introduction of surfactant F127 and activation temperature played a critical role in determining the textural properties and the surface chemistry (nitrogen and oxygen contents and chemical state) of the porous carbons. The electrochemical capacitive performance of the nitrogen-enriched HPCs was investigated. The contribution of nitrogen and oxygen functionalities was also discussed in great detail.

2. EXPERIMENTAL SECTION

2.1. Chemicals. 4-Cyanophenol (99%), urea, formaldehyde (37 wt % in water), absolute ethanol, and potassium hydroxide (KOH) were purchased from Tianjin Tianli Chemical Corp. Poly(ethylene oxide)/poly(propylene oxide)/poly(ethylene oxide) triblock copolymer ($EO_{106}PO_{70}EO_{106}$) Pluronic F127 was purchased from BASF Corp. All solvents and other chemicals were analytical reagent grade and were utilized without further purification.

2.2. Preparation of PBZ-Based HPCs. In a typical preparation, the composition was F127:urea:4-cyanophenol:formaldehyde:EtOH = 0.005:1:1:4:32.6 (molar ratio). To a 250 mL three-neck round-bottomed flask equipped with a magnetic stirrer, a thermometer, and a reflux condenser were added urea (4.0 g) and formaldehyde (5.0 g), and the resulting mixture was gradually heated to 90 °C for 30 min and then cooled to room temperature, denoted as solution A. F127 (4.2 g) and 4-cyanophenol (4.0 g) were dissolved in absolute ethanol (50.0 g) and stirred for 60 min, denoted as solution B. Then solution B was added into solution A and heated under reflux at 90 °C for 6 h. After cooling to room temperature, the reaction mixture was poured into dishes to evaporate ethanol at room temperature for 12 h. The obtained benzoxazine monomer together with surfactant F127 mixtures was heated stepwise in an oven at 100, 150, 180, 220, and 250 °C for 4 h, respectively. Then, the cured PBZ containing surfactant F127 was further carbonized under a nitrogen atmosphere by heating at 600 °C for 5 h with a ramp rate of 1 °C min^{-1}. Then, the obtained carbonized material, named HPC-0, was thoroughly mixed in an aqueous KOH solution in a weight ratio of KOH:carbonized sample = 2:1, followed by water evaporation at 120 °C. The activation process was carried out at 600, 700, or 800 °C for 1 h in a tube furnace under flowing nitrogen with a ramp rate of 3 °C min^{-1}. The products were repeatedly washed with 1 M HCl and deionized water until the pH value of the filtrate reached about 7 and dried at 110 °C for 12 h. The obtained samples were named HPC-*x*, where *x* represents the activation temperature. For comparison, the sample named NPC-600 was prepared without adding F127 and activated by KOH at 600 °C.

2.3. Characterization. N_2 adsorption isotherms were measured using a Micromeritics ASAP2020 analyzer at 77 K. Before measurements were taken, all samples were degassed at 473 K for 12 h. The specific surface area was calculated by the Brunauer−Emmett−Teller (BET) method, and the micropore area and micropore volume were determined by the *t*-plot method. The density functional theory (DFT) model assuming cylindrical-shaped pores was utilized to obtain the pore-size distribution (PSD). The PSD was also calculated based on the Barrett−Joyner−Halenda (BJH) model for mesopores. Scanning electron microscopy (SEM) investigations were carried out with a JEOL JSM-700 microscope instrument at an accelerating voltage of 10.0 kV. X-ray photoelectron spectroscopy (XPS) spectra were obtained on an AXIS Ultra DLD spectrometer with an excitation source of Mg Kα (1486.6 eV). Elemental analysis was performed by an Elementar Vario Macro EL Cube microanalyzer. Fourier transform infrared (FTIR) spectroscopy was carried out using a Bruker Vertex70 spectrometer over the wavenumber range of 4000−400 cm^{-1}. X-ray diffraction (XRD) patterns were obtained on a X-ray diffractometer (Bruker D8) with Cu Kα radiation (λ = 0.15406 nm). Raman spectra were obtained at ambient temperature on a Nanofinder 3.0 Raman spectrometer (Tokyo Instrument) using a visible laser beam of 488 nm as the excitation source. The direct-current electrical conductivity (σ) of the HPCs was tested by the four-point probe method on a four-point probe meter (RTS-8, Guangzhou, China) at room temperature. A round HPC tablet was fabricated by pressing (~20 MPa) 50 mg of the HPC powders with a tablet compression machine. The thickness and diameter of the round tablet were tested using a vernier caliper.

2.4. Electrochemical Measurements. Electrochemical measurements were performed using a three-electrode system and a two-electrode system. In a three-electrode system, platinum wire and Hg/HgO electrodes were used as the counter and reference electrodes, respectively. The powder of nitrogen-containing porous carbons (80 wt %), acetylene black (10 wt %), and poly(tetrafluoroethylene) (10 wt %) were mixed and stirred adequately. The mixture was pressed on a nickel foam current collector at a pressure of 10 MPa with the ratio of the mass and area at 10 mg cm^{-2}. Cyclic voltammetry (CV) and galvanostatic charge/discharge (GCD) behavior were tested in an electrolyte of 6 M KOH, and the potential window was chosen in the range of −0.9 to 0 V. The electrochemical impedance measurements were performed in a frequency range from 100 kHz to 10 mHz with an alternating-current amplitude of 10 mV. In a two-electrode system, one electrode was the test electrode, and the other electrode with nearly the same weight and size was the counter electrode. The cell consisted of the two electrodes sandwiched together, separated by a polypropylene membrane. CV and GCD behavior were also measured in a 6 M KOH electrolyte. All of the electrochemical tests were performed using a CHI 660C instrument (Shanghai Chenhua Apparatus Co. Ltd.) at room temperature.

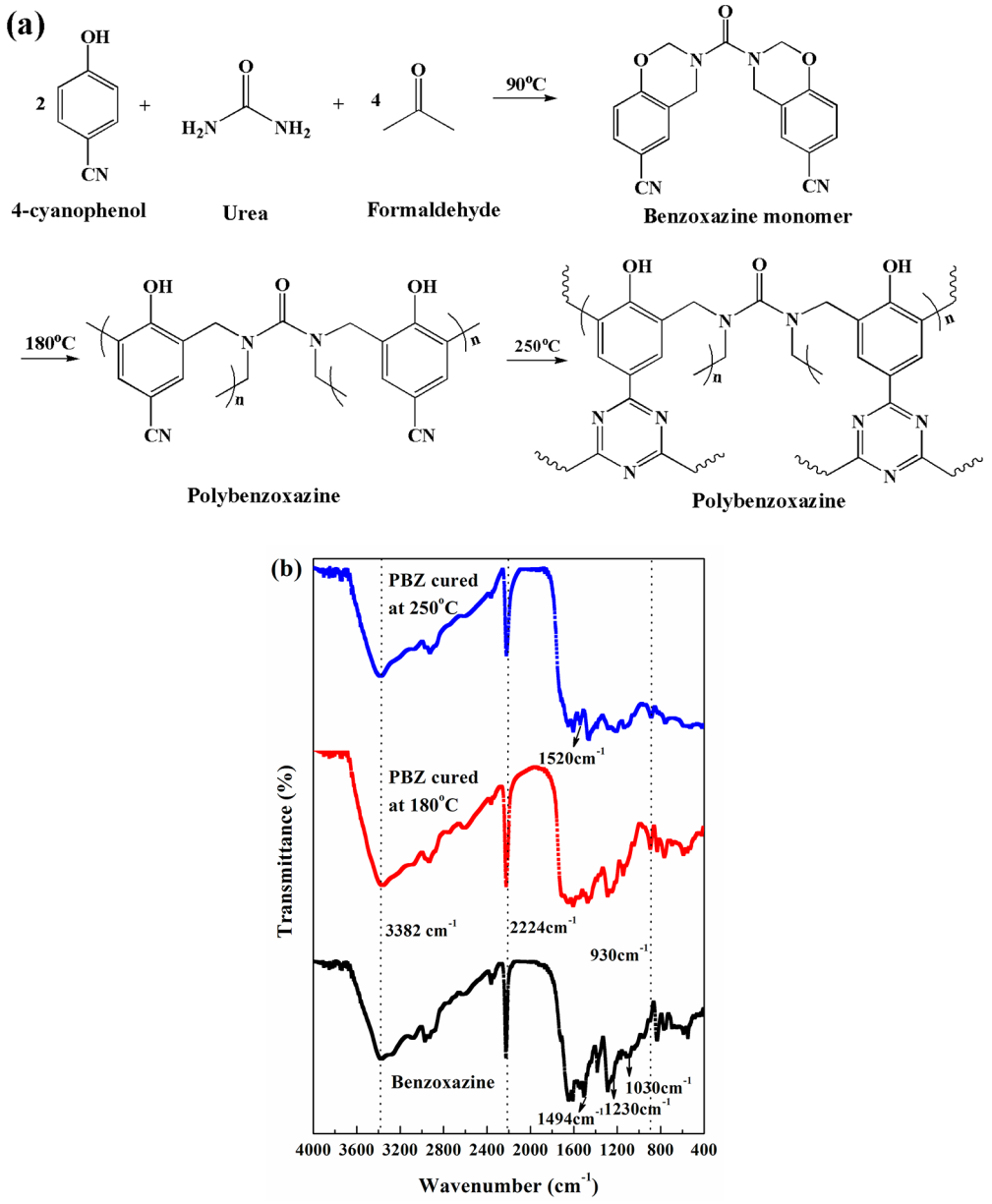

Figure 1. (a) Chemical reaction of the monomer synthesis, thermally activated ring-opening polymerization, and cross-linked structure of benzoxazines. (b) FTIR spectra of the benzoxazine monomer and PBZs cured at 180 and 250 °C.

The specific capacitance obtained from GCD cycling experiments in a three-electrode system was calculated by the following equation:

$$C_g = i\Delta t(m\Delta V)$$

where i is the constant discharging current, Δt is the discharge time, ΔV is the voltage window (in the present work, $\Delta V = 0.9$ V), and m is the mass of active materials loaded in the working electrode.

The specific capacitance for a single electrode in a two-electrode system was also calculated from the discharge curve according to the following equation:

$$C_g = 4i\Delta t(m\Delta V)$$

where i is the constant discharging current, Δt is the discharge time, ΔV is the voltage window, and m is the total mass of active materials loaded in two electrodes.

3. RESULTS AND DISCUSSION

3.1. Structure and Morphology Characterization. In order to obtain nitrogen-enriched HPCs, a novel precursor, a benzoxazine with nitrile functionalities, was synthesized via a solution method by using urea and 4-cyanophenol as the carbon and nitrogen sources, respectively. The synthesis reaction mechanism and thermally activated ring-opening polymerization reaction of benzoxazine are shown in Figure 1a. The benzoxazine monomer was first synthesized through Mannich condensation of 4-cyanophenol, urea, and formaldehyde without the addition of any catalyst. Then, a ring-opening polymerization reaction on the benzoxazines took place to form oxazine rings at temperatures between 180 and 250 °C. During the curing procedure, the polymerizable cyano groups in the benzoxazine could be further transformed into triazine rings through polymerization reactions, which formed an extra, extended 2D framework to further increase the cross-

linking density of PBZ.[27] Therefore, such a developed 3D framework of PBZ ensures its excellent thermal stability and high char yield after carbonization and activation at high temperature, as shown in Table 1. For the purpose of creating a certain amount of mesopores, the soft-templating agent (surfactant F127) dissolved in ethanol was introduced into a benzoxazine solution to obtain a mesotructured surfactant/polymer composite via the solvent-evaporation-induced self-assembly method.[28] Then, the composites were transformed into mesoporous carbon HPC-0 after decomposition of the soft-templating agent at 600 °C for 5 h. Furthermore, the chemical activation method under mild activation conditions (in a weight ratio of KOH:carbonized sample = 2:1 for 1 h) was applied to improve its micropore porosity with an interconnected pore structure.

Table 1. Yield and Textural Properties of the Samples

sample	S_{BET} ($m^2\ g^{-1}$)	S_{micro} ($m^2\ g^{-1}$)	V_{total} ($cm^3\ g^{-1}$)	V_{micro} ($cm^3\ g^{-1}$)	V_{micro}/V_{total} (%)	yield[a] (wt %)
HPC-0	178.5	112.7	0.13	0.09	69.2	75.7
NPC-600	954.8	857.1	0.45	0.40	88.7	67.4
HPC-600	1097.3	974.5	0.53	0.42	79.2	57.6
HPC-700	1526.5	1345.8	0.73	0.51	69.9	51.3
HPC-800	1555.4	997.8	0.73	0.45	62.4	45.5

[a]Yield (wt %) = (dry carbon material mass/precursor mass) × 100.

The FTIR spectra of the benzoxazine monomer and PBZs, which were cured at 180 and 250 °C for 4 h, are shown in Figure 1b, respectively. The broad peak at about 3382 cm^{-1} belongs to the OH stretching mode of the phenolic hydroxyl group. The characteristic peaks at 930 and 1494 cm^{-1} correspond to the oxazine ring. The band at 1230 and 1030 cm^{-1} can be linked to the presence of the asymmetric and symmetric stretching of C−O−C of the benzoxazine ring in the monomer structure, respectively.[29] The peak at 2224 cm^{-1} for the monomer is assigned to the cyano group. The intensity of the band at 2224 and 930 cm^{-1} decreased evidently with an increase of the temperature from 180 to 250 °C, indicating the gradually disappearance of the cyano group and the increase of the extent of ring opening of the monomer at high curing temperature, respectively. Besides, a new characteristic peak at 1520 cm^{-1} appeared for PBZs cured at 250 °C, which belongs to the triazine.[30] It can be ascribed to the transformation of cyano groups into triazine at 250 °C. These results prove the formation of a novel nitrile-functionalized benzoxazine and corresponding PBZ.

The SEM images of the obtained materials are shown in Figure 2. It can be seen that the precursor HPC-0 is composed of many irregular microparticles of about several hundreds of nanometers to a few micrometers in diameter (Figure 2a). Such loose structures are beneficial for chemical activation by KOH to develop the microporosity. NPC-600 exhibits a rough surface and no obvious cavities or macropores (Figure 2b). However, the surface morphologies of HPC600−HPC-800, which were activated at different activation temperatures, obviously have many voids and significant macropores with pore sizes over 0.5 μm (Figure 2c−e), which are probably caused by the release of residual gases during the activation process at high temperature. The sample HPC-600 shows independent and shallow macropores. As the activation temperature increased from 600 to 800 °C, the pore walls evidently became thinner and more macropores developed (Figure 2d,e) on the surface of the carbon network and even interconnected with each other, which might serve as ion-buffering reservoirs and give a decreased diffusion distance.

In order to investigate the development of porosity by a soft-templating method and KOH activation at different temperatures, N_2 adsorption/desorption isotherms of HPCs were obtained, as shown in Figure 3a. HPC-0 shows a type IV isotherm with an obvious hysteresis loop, implying the presence of mesopores. Figure 3b confirms that HPC-0 has a narrow mesopore size distributed between 2.0 and 2.1 nm. It is noticeable that the amount of the soft-templating agent F127 that was introduced into the synthetic system was limited. Thus, the mesopore porosity of HPC-0 is only 30.8%, and the mesopore surface area is as low as 178.5 $m^2\ g^{-1}$ (Table 1).

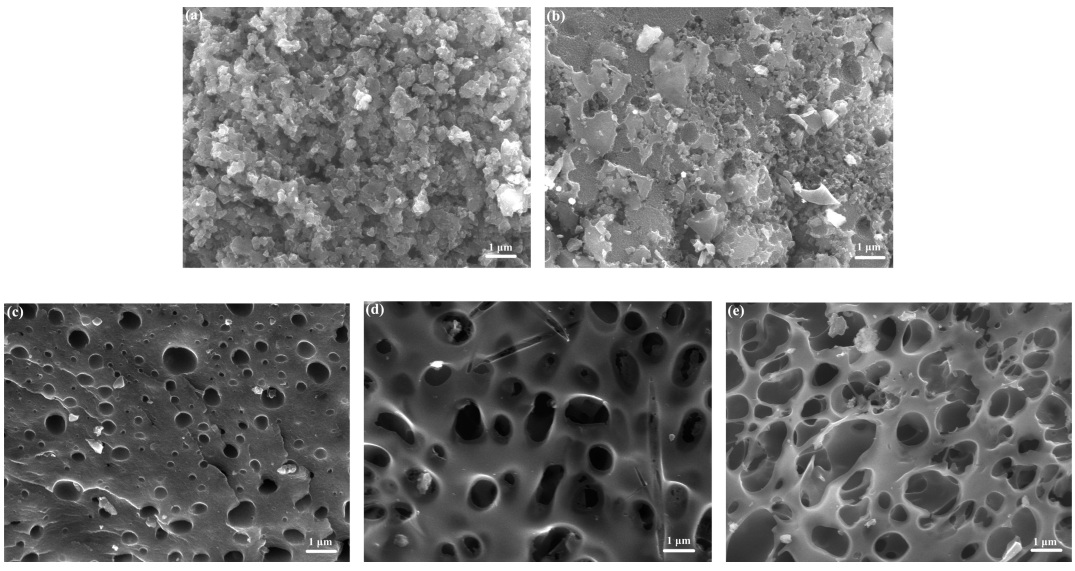

Figure 2. SEM images of (a) HPC-0, (b) NPC-600, (c) HPC-600, (d) HPC-700, and (e) HPC-800.

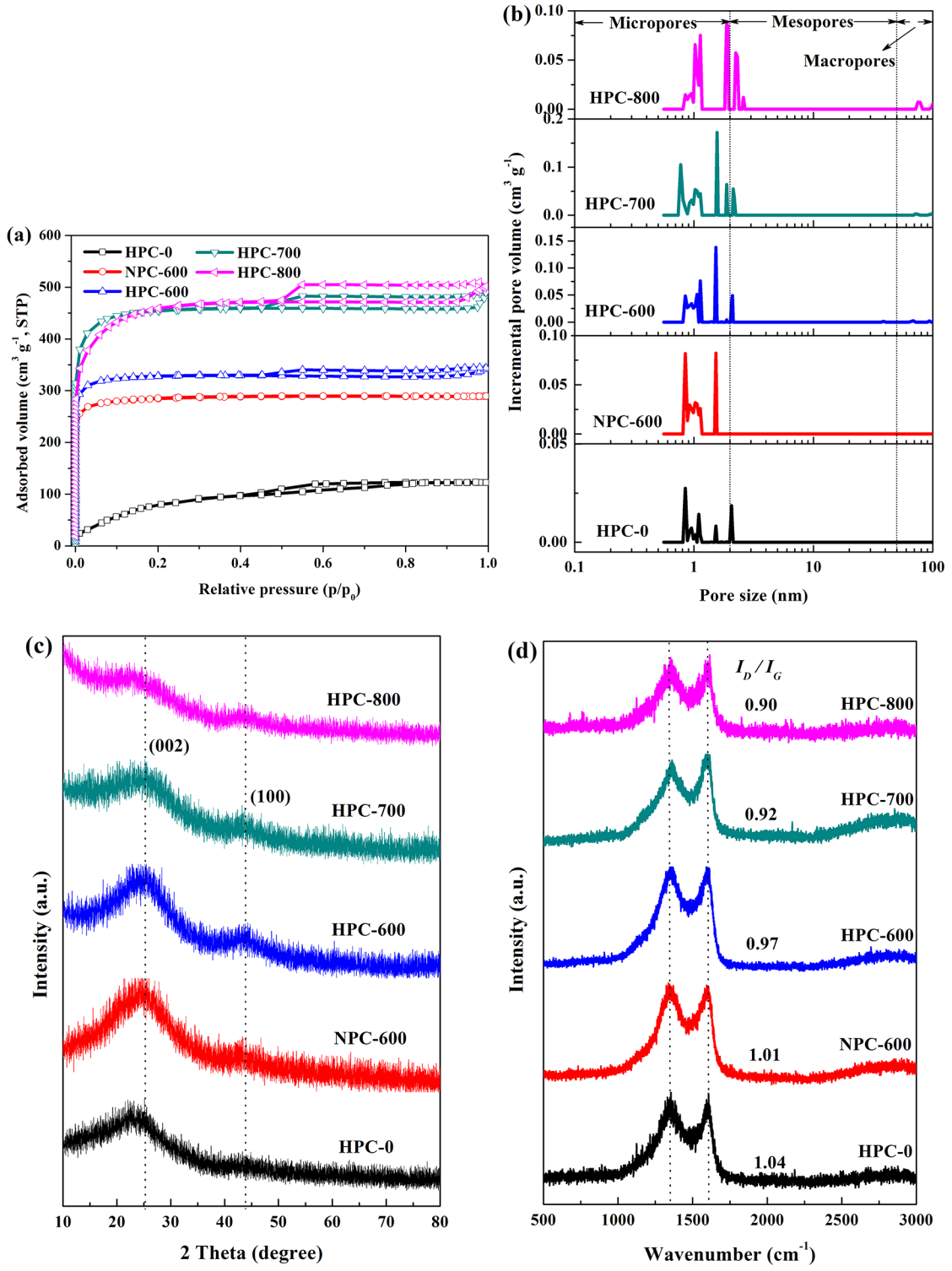

Figure 3. (a) N_2 adsorption isotherms. (b) PSDs obtained by the DFT method of all samples. (c) XRD patterns and (d) Raman spectra of all samples.

NPC-600 exhibits type I isotherms, indicating typical microporous carbon materials. Compared with HPC-0, no obvious meso/macropores can be found in NPC-600 from its PSD curve. This proves that the mesopores in HPC-0 were successfully produced by a soft-templating method, which arose from decomposition of surfactant F127 during the carbonization process. For samples HPC-600, HPC-700, and HPC-800, their isotherms all show type IV characteristics with similar hysteresis loops observed at relative pressures p/p_0 of ca. 0.45−1.0, suggesting the presence of mesopores. A sharp rise of the N_2 isotherm was also observed at low relative pressures (p/p_0 = 0.01), indicating the existence of a large number of micropores. The obvious sharp peaks at high relative pressure (p/p_0 > 0.9) denote the existence of macropores, which is consistent with the results of the SEM images. In a word, HPC-600, HPC-700, and HPC-800 exhibit hierarchical porous

dx.doi.org/10.1021/am504564q | ACS Appl. Mater. Interfaces 2014, 6, 15583−15596

Table 2. Elemental and XPS Analysis and Electrochemical Properties of the Samples

	elemental analysis (wt %)				XPS analysis (atom %)			C_g (F g^{-1})	
sample	C	H	N	O	C	N	O	1 A g^{-1}	40 A g^{-1}
HPC-0	78.35	2.32	6.26	13.07	81.21	5.89	12.90	48.0	
NPC-600	79.28	2.25	4.82	13.65	83.35	4.27	12.38	254.4	63.8
HPC-600	80.96	1.47	5.19	12.38	84.10	4.88	11.02	375.4	231.1
HPC-700	82.23	0.87	4.55	12.35	85.35	4.16	10.49	279.7	133.3
HPC-800	85.10	0.65	3.64	10.61	87.23	3.27	9.50	641.6	443.0

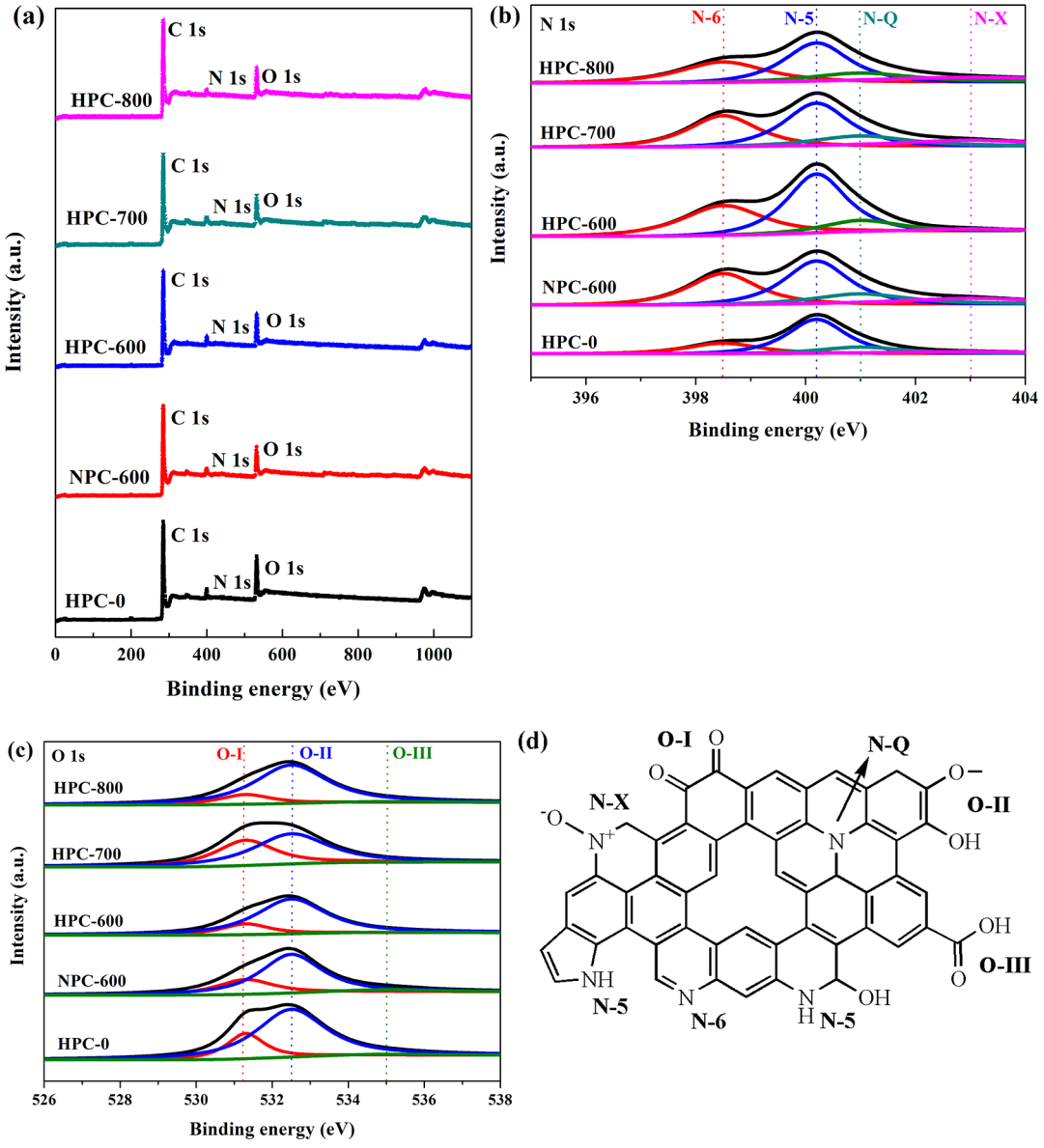

Figure 4. XPS spectra of all samples: (a) survey spectra; (b) N 1s; (c) O 1s; (d) nitrogen and oxygen species of the carbon materials.

structures: abundant micropores, limited mesopores, and a few macropores. Compared with NPC-600, the micropore size distribution of HPC-600 became wider as a result of the introduction of surfactant F127. This was probably caused by KOH corrosion with more accessible pore channels in the precursor HPC-0. Remarkably, the average mesopore size of HPC-600 maintained about 2.1 nm, revealing that the mesostructure of HPC-0 was not influenced by chemical activation. Besides, the activation temperature also has a remarkable impact on the pore structure. As the KOH activation process deepened at higher temperature, new micropores were generated and the ultramicropores were widened, resulting in higher surface area and total pore volume with a lower fraction of the micropore volume for HPC-800 (see Table 1). The average mesopore size increased slightly from 2.1 to 2.3 nm with an increase of the activation temperature from 600 to 800 °C, indicating that the mesopores were enlarged by KOH etching under severe activation conditions. Such a trend for the mesopore structure evolution of the HPCs was further demonstrated by the PSDs obtained

Table 3. XPS Peak Positions and Relative Surface Concentrations of Oxygen and Nitrogen Species Obtained by Fitting the N 1s and O 1s Spectra

sample	N-6 (398.5 eV)	N-5 (400.2 eV)	N-Q (401 eV)	N-X (403 eV)	O-I (531.3 eV)	O-II (532.5 eV)	O-III (535.0 eV)
HPC-0	21.84	58.10	14.41	5.66	23.78	73.88	2.34
NPC-600	33.38	42.95	13.82	9.85	25.27	70.18	4.54
HPC-600	35.02	50.66	12.11	2.21	18.52	79.97	1.51
HPC-700	33.31	42.82	13.85	10.02	40.48	58.07	1.45
HPC-800	30.77	43.40	15.00	10.83	16.02	81.73	2.25

by the BJH method (see Figure S1 in the Supporting Information, SI). Furthermore, macropores with size ranging from 60 to 100 nm for HPC-600, HPC-700, and HPC-800 were created by KOH corrosion and volatilization of unstable nitrogen and oxygen functionalities at high temperature. Because of PBZs' high chemical and thermal stability, all obtained carbon materials exhibit high yield (more than 45%), as shown in Table 1.

The graphitic property of the carbon samples is investigated by wide-angle XRD patterns and Raman spectra. The XRD patterns of NPC-600 and the HPCs are given in Figure 3c. Two typical, broad diffraction peaks are observed at around 2θ = 25 and 44°, which belong to diffraction of the (002) and (100) planes of the hexagonal graphitic carbon, respectively.[31] This indicates that all of the nitrogen-containing porous carbons are amorphous and nongraphitized. HPC-0, NPC-600, and HPC-600 prepared at 600 °C have similar, broad diffraction peaks. However, when the activation temperature increased from 600 to 800 °C, the intensity of the (100) peak was gradually enhanced, implying the improvement of the graphitization degree of HPC-800. Figure 3d shows the Raman spectra of all samples. Two strong peaks at 1350 cm^{-1} (D band) and 1595 cm^{-1} (G band) are observed for all carbon materials, respectively. In detail, the D band refers to the disordered and imperfect structures in the carbonaceous materials, and the G band is related to the vibration of a sp^2-hybridized carbon in the graphite crystallites.[32] The samples HPC-0, NPC-600, and HPC-600 obtained at 600 °C exhibit an intense D band, implying the existence of abundant defects, such as a large number of nitrogen and oxygen atoms. The intensity ratio of D and G bands (I_D/I_G) represents the graphitic degree of the carbon materials.[33,34] The values of I_D/I_G are 1.04, 1.01, 0.97, 0.92, and 0.90 for HPC-0, NPC-600, HPC-600, HPC-700, and HPC-800, respectively. This reveals that the introduction of surfactant F127 or chemical activation resulted in small changes of the graphitic degree of the carbon materials because of the similar chemical compositions and structures of HPC-0, NPC-600, and HPC-600. However, as the thermal treatment temperature increased from 600 to 800 °C, the vibration of the D band became weaker and I_D/I_G for HPC-600−HPC-800 decreased, indicating the higher degree of graphitization and a decrease of the disordered structure for HPC-800. This can be attributed to the loss of nitrogen and oxygen species at high activation temperature. These results are in good agreement with XRD analysis.

The chemical compositions of the obtained carbon materials are shown in Table 2. It can be seen that all samples contain relatively high nitrogen species (3.64−6.26 wt %) and oxygen species (10.61−13.65 wt %). These heteroatoms can only be derived from the intrinsic nitrogen and oxygen components in the nitrile-functionalized PBZs (see Figure 1). More importantly, the nitrogen and oxygen atoms in the carbon matrix are considered to effectively improve the wettability and electrical conductivity of the carbon-based materials, facilitate the accessibility of the electrolyte ions, and enhance the capacitance performance.[18,19] The contents of the nitrogen and oxygen atoms in HPC-600−HPC-800 decreased evidently with an increase of the activation temperature because of the poor thermal stability of the nitrogen and oxygen species at high temperature. The chemical state of the nitrogen and oxygen species on the surface of the carbon materials was further studied by XPS analysis (Figure 4). Four types of nitrogen species can be distinguished on all sample surfaces: pyridinic nitrogen (N-6 at 398.5 eV), pyrrolic or pyridonic nitrogen (N-5 at 400.2 eV), quaternary nitrogen (N-Q at 401 eV), and oxidized nitrogen (N-X at 403 eV), as shown in Table 3 and Figure 4d.[35] This reveals that the N-6 and N-5 species are predominant (more than 74% of the total nitrogen atoms) for all samples, which might be derived from the transformation of amide groups and triazine rings in PBZs after thermal treatment. Such high contents of N-6 and N-5 in PBZ-based nitrogen-containing porous carbons are much higher than many other nitrogen-rich carbon materials.[17−19] More importantly, N-6 and N-5 are considered to be electrochemically active in an alkaline aqueous solution to provide main pseudocapacitance, which is significant for nitrogen-doped carbon materials to increase the capacitance.[13] Besides, the presence of N-Q, which are inset into the carbon matrix and bonded to three carbon atoms, can effectively benefit electron transfer and improve the conductivity of carbonaceous materials.[36] Thus, it can be inferred that HPC-800 with the highest N-Q content exhibits better conductivity than other samples. The conclusion was further proved by the electrical conductivity measurement results. The electrical conductivity σ values for HPC-0, NPC-600, HPC-600, HPC-700, and HPC-800 are 2.86, 3.22, 3.24, 3.39, and 3.44, respectively, which are much higher than those of many activated carbons and ordered mesoporous carbons without incorporating any heteroatoms (0.2−2 S cm^{-1}).[2,5] This can be attributed to the local graphite-like microstructure and large amount of nitrogen and oxygen species in the carbon network. The electrical conductivity evidently enhances with an increase of the N-Q content (see Table 3). Moreover, an increase of the degree of graphitization also results in an increase of the conductivity of the nitrogen-enriched porous carbons. Thus, HPC-800, possessing the highest N-Q content and highest degree of graphitization, shows the best electrical conductivity among the five samples. Besides, with an increase of the activation temperature, the percentage of N-Q increased but N-X evidently decreased. This reveals that N-Q was more thermally stable than N-X and that N-5 and N-6 were partially converted into N-Q at high temperature. Furthermore, compared with NPC-600, the slightly higher nitrogen content in both bulk and surface for HPC-600 can be attributed to decomposition of the surfactant F127 together with the oxygen species in the precursor during thermal treatment.

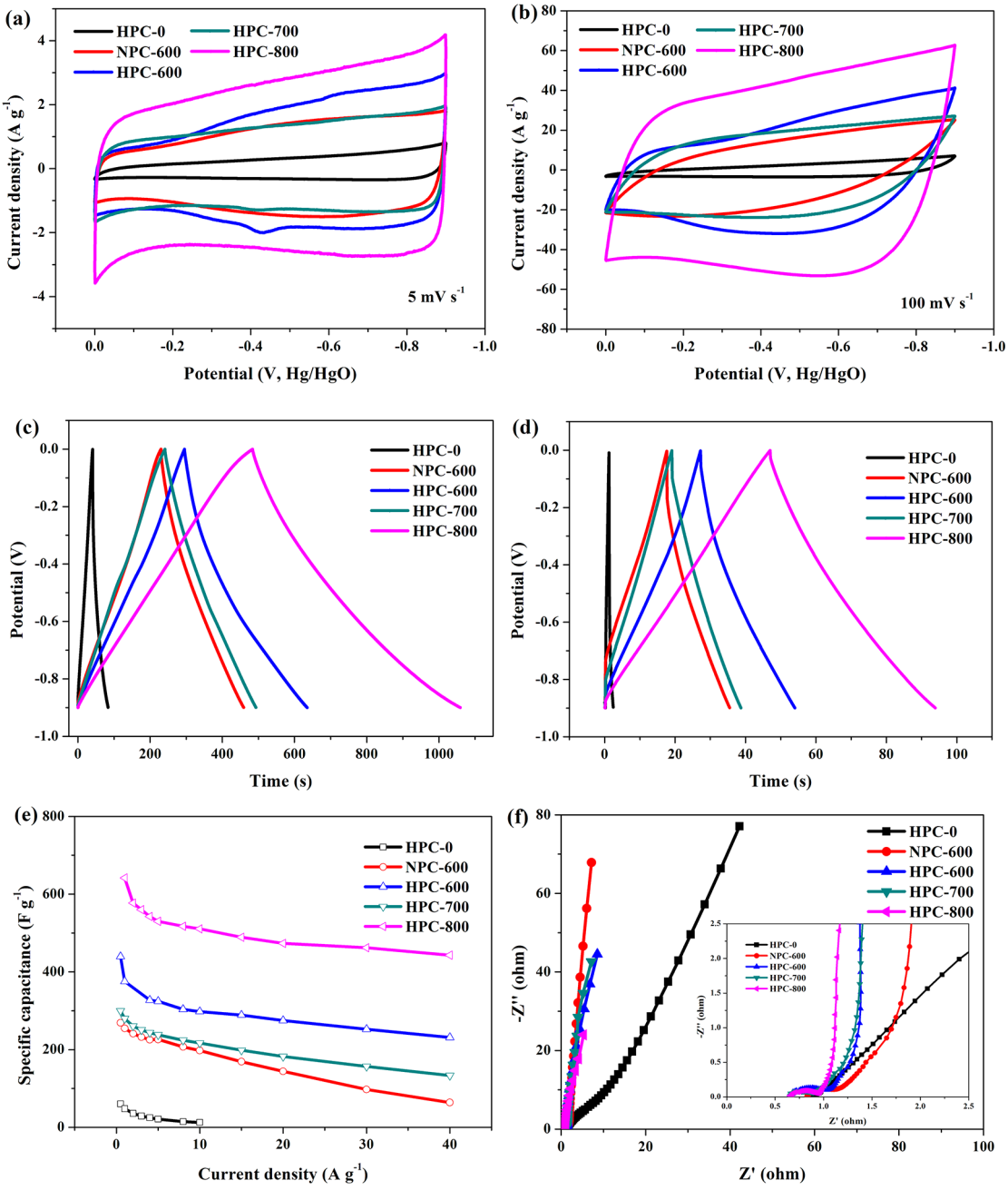

Figure 5. Electrochemical performance of all HPC electrodes measured in a three-electrode system: CV curves for all samples at scan rates of (a) 5 and (b) 100 mV s^{-1}. GCD curves for all samples at current densities of (c) 1 and (d) 10 A g^{-1}. (e) Specific capacitance as a function of the discharge current density for all samples. (f) Nyquist plots in the frequency range of 10 mHz to 100 kHz.

The O 1s spectra of HPCs can be resolved into quinone (O-I), phenolic hydroxyl or ether (O-II), and carboxyl (O-III) peaks centered at 531.3, 532.5, and 535.0 eV, respectively (Table 3 and Figure 4d). Among these three oxygen functional groups, quinone groups in the carbon matrix are not electrochemically active in the reversible redox reactions in an alkaline medium.[37] Instead, reduction of O-II and deprotonation of O-III exhibited quasi-reversible pseudocapacitances.[38,39] It is noticeable that all samples have high oxygen content (exceed 10 wt % according to the elemental analysis results) with extremely high O-II and O-III contents (exceeding 74 atom % of the total oxygen atoms), as shown in Table 3. Thus, the large amount of O-II, O-III, N-6, and, N-5 functionalities in the PBZ-based HPCs can generate great pseudocapacitance in a 6 M KOH aqueous electrolyte.[35] The influence of the textural properties and surface chemistry of the HPCs on the capacitance was further estimated by electrochemical characterization.

3.2. Electrochemical Measurements. The electrochemical performance of all nitrogen-containing porous carbons as electrode materials for supercapacitors was evaluated by a three-electrode system in a 6 M KOH aqueous electrolyte. Figure 5a shows typical CV curves of all five electrodes at a scan rate of 5 mV s^{-1}. It can be observed that all of them present a quasi-rectangular voltammogram shape at a low scan rate, exhibiting typical characteristics of EDLCs, indicative of them being excellent candidates as electrode materials.[40] The nonactivated carbon material HPC-0 exhibits the smallest

dx.doi.org/10.1021/am504564q | ACS Appl. Mater. Interfaces 2014, 6, 15583−15596

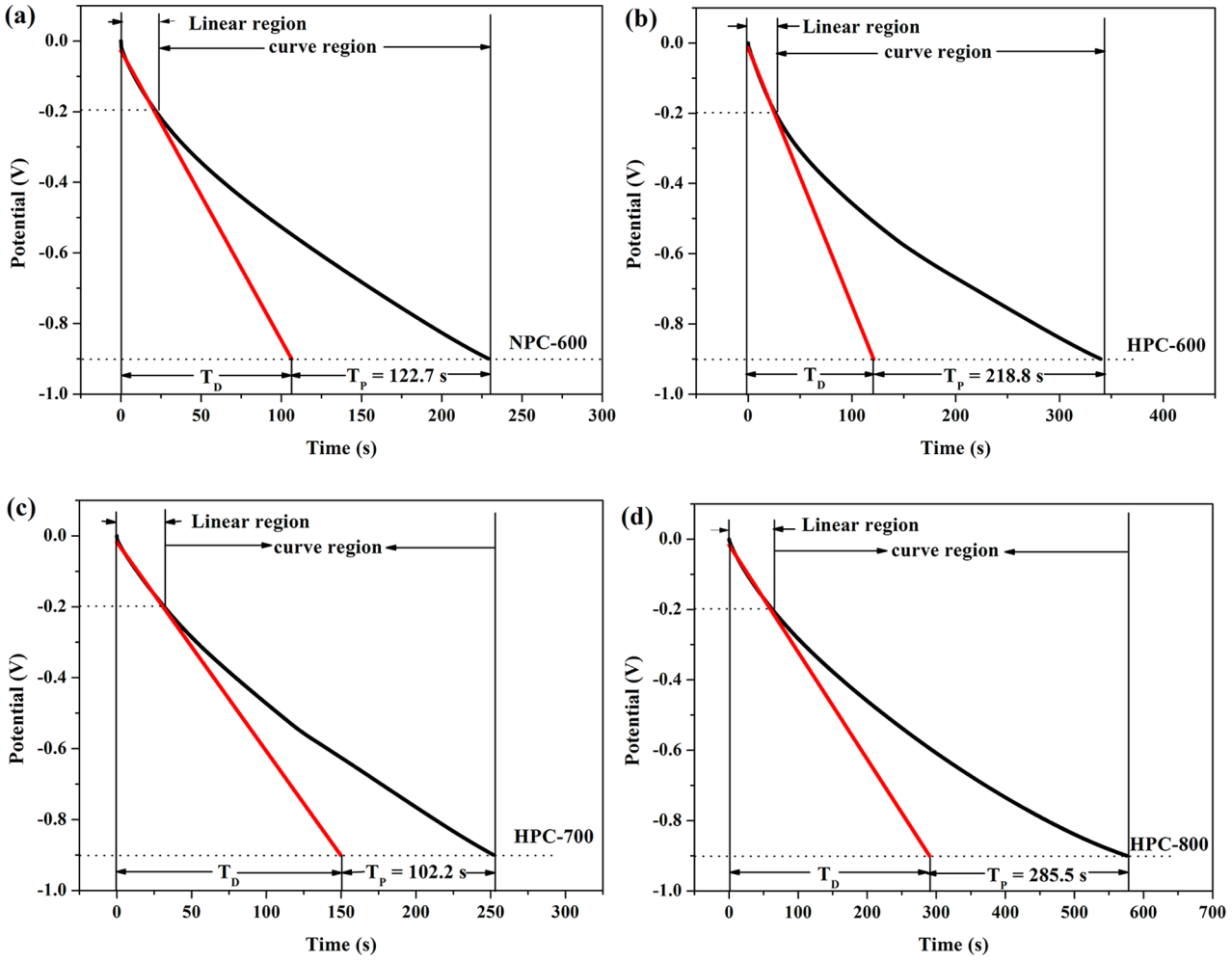

Figure 6. Discharge time of the pseudocapacitance parts of (a) NPC-600, (b) HPC-600, (c) HPC-700, and (d) HPC-800 electrodes at 1 A g^{-1}.

current density response compared with the KOH-activated carbons at the same scan rate, indicating the smallest specific capacitance of HPC-0. This can be attributed to its lowest specific surface area and thus a small electric double-layer (EDL) contribution. Noticeably, the CV curve for the HPC-600 electrode shows small oxidation and reduction peaks in addition to rectangular shape, indicating the existence of pseudocapacitive reactions.[41] This can be ascribed to its highest nitrogen content among the four KOH activated samples. However, other samples' CV curves exhibit no obvious evidence of redox peaks but broadened pseudopeaks, indicating that the great contribution of EDLC as well as the pseudocapacitance. Although HPC-0 contains the largest number of nitrogen and oxygen species in the five samples, the low specific surface area and less developed porosity of HPC-0 make it difficult for fast charge transfer during the Faradaic reactions and result in poor capacitive behavior. When the scan rate increases from 5 to 100 mV s^{-1}, the CV curves for the HPC-600−HPC-800 electrodes still remain a less rectangular shape (Figures 5b and S2 in the SI), implying good capacitive performance for quick charge/discharge operations. The broad pseudocapacitance peaks on the CV curves for HPC-600 ∼ HPC-800 electrodes can be ascribed to the combined contribution of the double-layer and Faradaic redox capacitances.[42] However, the CV curve for the NPC-600 electrode becomes seriously distorted at high scan rates, indicating that such a microporous carbon with narrow micropore size distribution is unfavorable for quick electrolyte ion diffusion. This confirms that the hierarchical pore structure is beneficial for fast ionic transportation and penetration within the macro/mesopore channels and adequate utilization of the interior surfaces through low-resistance pathways.[43] Thus, HPC-600−HPC-800 show improved capacitive performance in comparison with the carbonized sample HPC-0 and microporous carbon NPC-600.

Figure 5c clearly shows the GCD curves of all five electrodes at a current density of 1 A g^{-1}. It can be seen that GCD curves of all five electrodes are nearly linear and symmetrical with slight curvature, indicating good capacitive properties and electrochemical reversibility. The deviation to linearity for all GCD curves is typical of a pseudocapacitance contribution, which confirms the presence of Faradaic capacitance. Compared with the other four electrodes, the discharge curve of the HPC-0 electrode exhibits the shortest discharge time, and its capacitance is as low as 48.0 F g^{-1} at 1 A g^{-1}, which is consistent with the CV results. The NPC-600 electrode shows much shorter discharge time than the HPC-600 electrode. The presence of meso/macropores in HPC-600 not only makes the inner micropore surface more electrochemically accessible for electrolyte ions and more charges to be accumulated in the micropores but also facilitates the fast diffusion of electrolyte ions in the pore channels at high current densities. Moreover,

dx.doi.org/10.1021/am504564q | ACS Appl. Mater. Interfaces 2014, 6, 15583−15596

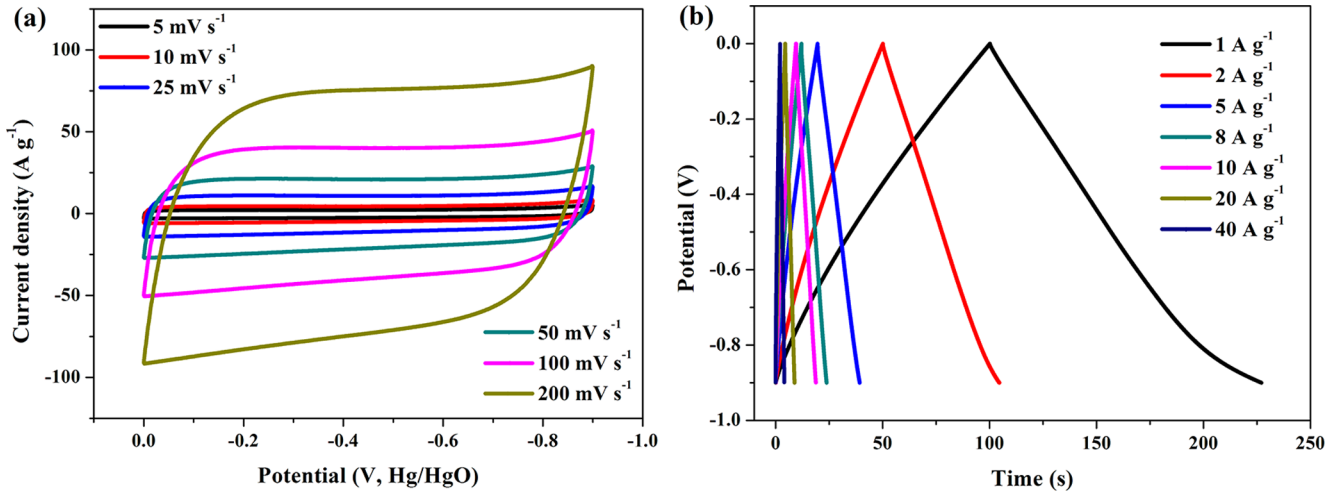

Figure 7. Electrochemical performance of the HPC-800 electrode measured in a two-electrode system. (a) CV curves at different scan rates. (b) GCD curves at different current densities.

the higher contents of electrochemically active N-6, N-5, O-II, and O-III functionalities for HPC-600 generate more pseudocapacitance than that of the NPC-600 electrode. Therefore, the specific capacitance of the HPC-600 electrode increases by 47.6% at 1 A g^{-1} and 262.2% at 40 A g^{-1} compared to the NPC-600 electrode at the same current densities, respectively (see Table 2). Compared with the HPC-600 electrode, a decrease of the discharge time with an increase of the activation temperature for the HPC-700 electrode can be attributed to a decrease of significant pseudocapacitance, which results from the loss of electrochemically active nitrogen and oxygen species for HPC-700. Even when the current density increases to 20 A g^{-1} (Figure 5d), the GCD curves for all five electrodes still maintain a nearly linear-like shape with evident IR drop. In detail, there is a much larger IR drop of the NPC-600 electrode than of the HPC-600 electrode at a high current density of 20 A g^{-1}. This indicates that the HPC-600 electrode has less overall resistance because of its wider micropore distribution and the presence of meso/macropores. Besides, the IR drops for HPC-600−HPC-800 electrodes become smaller with an increase of the activation temperature because of the higher fractions of meso/macropores.

In order to further investigate the contribution of the pseudocapacitance from nitrogen and oxygen functionalities to the total specific capacitance, the discharge curve can be divided into two parts because of the different extents of inflection at about −0.2 V in the GCD curve (Figure 6). The linear part of the time dependence of the potential (linear region) represents the EDLC. The other part of the discharge curve (curve region) is not strictly symmetrical and slightly distorted, which is considered to be the result of the combination of the EDLC and pseudocapacitance.[44] The extended lines of the linear parts are drawn in Figure 6 to calculate the pseudocapacitance by nitrogen and oxygen functionalities. T_D stands for the discharge time of the EDLC, and T_P stands for the discharge time of the pseudocapacitance. Therefore, the pseudocapacitances calculated from T_P of the NPC-600, HPC-600, HPC-700, and HPC-800 electrodes are 136.3, 243.1, 113.6, and 317.2 F g^{-1} at 1 A g^{-1}, which accounts for about 53.6, 64.8, 40.6, and 49.4% of the corresponding total capacitances, respectively. This confirms the pronounced contribution of pseudocapacitance for the nitrogen-enriched HPCs.

Figure 5e exhibits the specific capacitance as a function of the discharge current density for all samples. It can be seen that the specific capacitance of HPC-0 drops from 48.0 to 12.6 F g^{-1} with a decrease in the current density from 1.0 to 10 A g^{-1}, retaining only 26.2% of its initial specific capacitance. For the NPC-600, HPC-600, HPC-700, and HPC-800 electrodes, the values of the final specific capacitances at 40.0 A g^{-1} are 25.1, 61.6, 47.7, and 69.0% of the initial values at 1.0 A g^{-1}, respectively (see Table 2). This reveals that HPC-600−HPC-800 retain excellent capacitive behavior at high current densities, owing to their hierarchical porous structures and good electrical conductivity. However, the nonactivated carbon HPC-0 electrode and microporous carbon NPC-600 electrode show poor rate capability because of the less developed specific surface area and low porosity for HPC-0 and large diffusion resistance for NPC-600.

With an increase of the activation temperature, both HPC-600 and HPC-700 have similar pore structure and oxygen content, but the capacitance of the HPC-700 electrode with higher surface area dramatically decreases with a decrease of the nitrogen content at 1−40 A g^{-1}. The result is also consistent with the much smaller pseudocapacitance obtained from T_P for the HPC-700 electrode than that of the HPC-600 electrode. It can be further concluded that nitrogen functional groups play a more important role than oxygen functional groups in this work. Besides, compared with HPC-700, HPC-800 exhibits similar surface area, smaller micropore surface area and micropore volume, as well as lower bulk nitrogen content, but the HPC-800 electrode demonstrates the highest specific capacitances at all current densities (Figure 5e), resulting from its high specific surface area, an optimal PSD, abundant meso/macropores with highly accessible surface for more nitrogen and oxygen functional groups to provide large pseudocapacitance, high degree of graphitization, and superior electrical conductivity. This reveals that, except for the high content of the N-6, N-5, O-II, and O-III functional groups in the porous carbon materials, the accessibility of the nitrogen-doped carbon surface for the electrolyte ions also plays an important role in improving the pseudocapacitance.[45,46]

Figure 5f exhibits Nyquist plots of all five electrodes. The HPC-0 electrode shows a small semicircle at the frequency region and an inclined line at the low-frequency region, indicating poor capacitive performance and high ion-diffusion

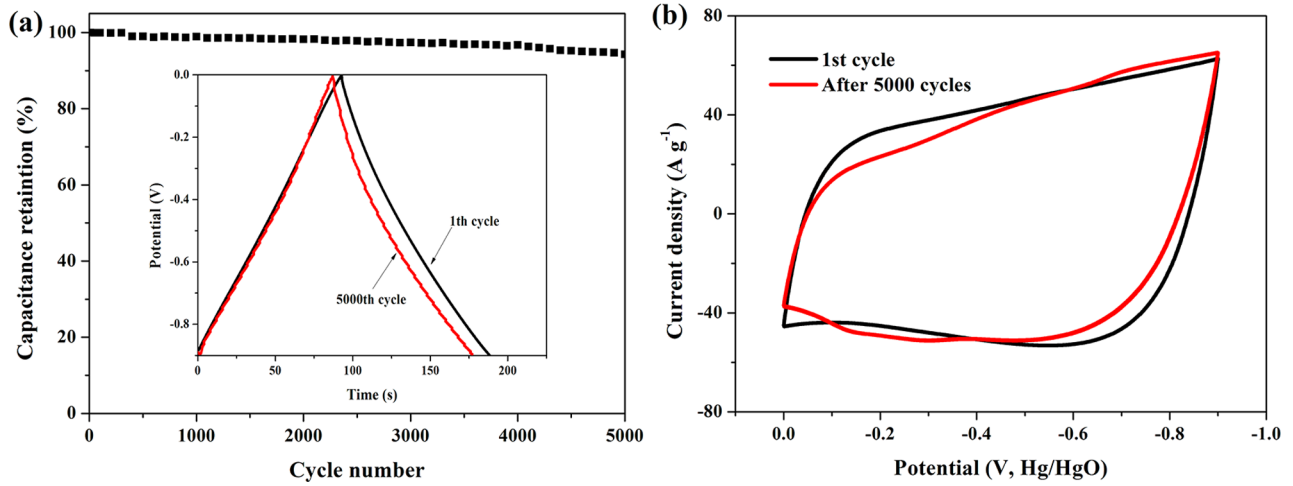

Figure 8. (a) Cycling stability of the HPC-800 electrode at a current density of 5 A g^{-1}. (b) CV curves of the 1st and 5000th cycles of the HPC-800 electrode at a scan rate of 100 mV s^{-1} in a three-electrode system.

Table 4. Comparison of the Specific Capacitance Parameters of Different Nitrogen-Containing Porous Carbons in 6 M KOH in the Literature

material	S_{BET} (m^2 g^{-1})	N %	C_g (F g^{-1})	C_g/S_{BET} (F m^{-2})	current density (A g^{-1})	ref
nitrogen-doped porous carbons from gelatin	3012	0.88	385	0.128	1.0	18
hierarchical nitrogen-doped porous carbon from endothelium corneum gigeriae galli	2149.9	2.04	198	0.092	1.0	19
nitrogen-enriched carbon from melamine mica	6	13.5	198	33	0.05	27
nitrogen-enriched carbon nanowires from polyaniline nanowires	641	7.04	327	0.510	0.1	50
nitrogen-containing hydrothermal carbon	571	4.4	220	0.385	0.1	51
nitrogen-doped ordered mesoporous carbon	537	13.10	227	0.423	0.2	52
nitrogen-doped porous carbon	128	14.12	224	1.75	1.0	53
nitrogen-doped porous nanofibers	562.51	7.22	202	0.359	1.0	55
NPC-600	954.8	4.82	254.4	0.266	1.0	this work
HPC-600	1097.3	5.19	375.4	0.342	1.0	this work
HPC-700	1526.5	4.55	279.7	0.183	1.0	this work
HPC-800	1555.4	3.64	641.6	0.412	1.0	this work

resistance of the nonactivated sample.[47] The NPC-600, HPC-600, HPC-700, and HPC-800 electrodes show a similar Nyquist plot shape, a depressed semicircle on the Z' axis at the high-frequency region, and a nearly straight line at the low-frequency region, indicating good capacitive behavior of the chemically activated samples. With an increase of the activation temperature, the shortened and less gradual sloping line at high-to-medium frequency for HPC-600−HPC-800 electrodes implies lower diffusion resistance,[48] which is attributed to the more developed meso/macropores at high activation temperature. On the basis of the same testing conditions, the diameter of the semicircle at high frequency refers to the charge-transfer resistance of the electrode materials, as shown in the inset of the expanded high-frequency region of Figure 5f.[49] The charge-transfer resistances for the HPC-0, NPC-600, HPC-600, HPC-700, and HPC-800 electrodes are 0.77, 0.93, 0.65, 0.61, and 0.38 Ω, respectively. This reveals that the HPC-800 electrode possesses the best ionic conductivity over the other samples because of its highest electrical conductivity and highest degree of graphitization. In addition, the transfer resistance of the HPC-600 electrode was much smaller than that of the NPC-600 electrode. This confirms that the introduction of surfactant F127 can effectively tailor the pore structure and thus facilitate the transfer and penetration of the electrolyte ions into the inner pores.

To better study the electrochemical behavior of the HPC-800 electrode as a real capacitor in a 6 M KOH solution electrolyte, a symmetrical two-electrode configuration was constructed. Figure 7a shows the CV curves of the HPC-800 electrode at different scan rates (5−200 mV s^{-1}) using a two-electrode system. This reveals that the current densities increase evidently with an increase of the scan rates, implying the good rate capacity. It is noticeable that there is a sharp peak at −0.9 V at a slow scan rate (5 mV s^{-1}), which is related to the redox reactions. The CV curve of the HPC-800 electrode still maintains a rectangular-like shape at a scanning rate as high as 200 mV s^{-1}, but the NPC-600, HPC-600, and HPC-700 electrodes exhibit distorted CV shapes due to increased electrical resistance (see Figure S3b in the SI). Moreover, the specific capacitances for a single HPC-800 electrode (563.9 and 347.9 F g^{-1} at 1 and 20 A g^{-1}, respectively) calculated from the discharge curve in Figure 7b by using a two-electrode setup are slightly smaller than the values at the same current densities by using a three-electrode setup because of the different measurement methods (see Table S1 in the SI). It also demonstrates a good rate capability with a high capacitance retention ratio of 61.7% at 40 A g^{-1} for the HPC-800 electrode. Furthermore, the HPC-800 electrode exhibits good electric conductivity because its IR drop is minimal at a high current density of 10 A g^{-1} among the five HPC electrodes (see Figure

S3d in the SI), which is consistent with the electrical conductivity measurement results.

In order to evaluate the cycling stability of the HPC-800 electrode, GCD studies were performed at a current density of 5.0 A g^{-1} between −0.9 and 0 V in the 6 M aqueous KOH electrolytes using a three-electrode system. After 5000 cycles, the specific capacitance of the HPC-800 electrode decreased from 530.2 to 500.0 F g^{-1}, with a capacitance retention ratio of 94.3% (Figure 8a), indicative of excellent long-term cycling durability. The cycling durability of theHPC-800 electrode can be confirmed by the integral areas surrounded by the CV curves of the 1st and 5000th cycles at a scan rate of 100 mV s^{-1}, as depicted in Figure 8b.

Table 4 shows a comparison of the specific capacitances C_g and the interfacial capacitance C_s ($C_s = C_g/S_{BET}$) of HPCs prepared from PBZs with other nitrogen-enriched porous carbons in 6 M KOH in the literature. The specific capacitances of the HPC-600 and HPC-700 electrodes in this work are comparable to those previously reported for the nitrogen-enriched porous carbons (Table 4). Remarkably, the specific capacitance of the HPC-800 electrode is the highest at present compared with many nitrogen-containing porous carbon materials previously reported.[18,19,50−53] Furthermore, according to the theoretical capacitance per area of 0.20 F m^{-2} for activated carbons as electrode materials,[54] the theoretically calculated capacitance values for the NPC-600 and HPC-600−HPC-800 electrodes cannot exceed 191.0, 219.5, 305.3, and 311.1 F g^{-1}, respectively. This indicates that, except for HPC-700, at least 24.9, 41.5, and 51.5% of the total specific capacitances for the NPC-600, HPC-600, and HPC-800 electrodes were derived from the contribution of pseudocapacitance by the large number of nitrogen and oxygen functional groups in the carbon matrix, respectively. These estimated values are comparable to the calculated results obtained from the discharge time of the pseudocapacitance.

In a word, the HPC-800 electrode shows extremely high specific capacitance and outstanding rate capability and cycling stability because of the following superior properties: (1) high specific surface area to provide enough surface sites to form EDL; (2) the optimal hierarchical pore structure with high fraction of meso/macropores, which provides more accessible micropore surface, reduces diffusion resistance, and facilitates fast ionic transportation in the pore channels; (3) the existence of high contents of electrochemically active nitrogen and oxygen functional groups, which not only improves the hydrophilicity and wettability of the HPC and its affinity with the electrolyte but also participates in reversible redox reactions and generates pronounced pseudocapacitance; (4) high graphitization degree and good electrical conductivity, which is also critical for high-performance capacitors.

4. CONCLUSIONS

Novel nitrogen-enriched HPCs were for the first time successfully synthesized from a novel PBZ by a soft-templating method together with KOH activation. The introduction of a soft-templating agent and chemical activation temperature has a great influence on the textural properties and the surface chemistry of HPCs and thus influenced their capacitive performance. The sample HPC-800 electrode obtained by KOH activation at 800 °C exhibits a maximum specific capacitance of 641.6 F g^{-1} at a current density of 1 A g^{-1} in a 6 M KOH electrolyte. Moreover, its specific capacitance can still retain 443.0 F g^{-1} at 40 A g^{-1} with a capacitance retention ratio of 69%, which is ascribed to its high surface area, optimal PSD, abundant nitrogen and oxygen functional groups attached to the carbon network, high graphitization degree, and electrical conductivity. It is worth noting that no obvious capacitance loss is observed over 5000 charge/discharge cycles, clearly demonstrating good cycling durability. The nitrogen-enriched HPC represents an alternative promising candidate for high-performance electrode materials for supercapacitors.

■ ASSOCIATED CONTENT

Supporting Information

PSDs, electrochemical and electrochemical capacitive performances of all HPC electrodes, and specific capacitances of the samples. This material is available free of charge via the Internet at http://pubs.acs.org.

■ AUTHOR INFORMATION

Corresponding Author

*Tel.: 86 351 4250292. Fax: 86 351 4250292. E-mail: likx@sxicc.ac.cn.

Notes

The authors declare no competing financial interest.

■ ACKNOWLEDGMENTS

This work is supported by the National Natural Science Foundation of China (No. 51002166, 51172251, and 51061130536), International Cooperation Project of the Ministry of Science and Technology (No. 2010DFB90690-4), International Cooperation Project of the Shanxi Province (No. 2013081016), the Shanxi Province Science and Technology Developing Project (20120313006-4), and Shanxi Province Science and Technology Industrialization Project (2013071051).

■ REFERENCES

(1) Winter, M.; Brodd, R. J. What Are Batteries, Fuel cells, and Supercapacitors? *Chem. Rev.* **2008**, *104*, 4245−4270.

(2) Zhang, L. L.; Zhao, X. S. Carbon-Based Materials as Supercapacitor Electrodes. *Chem. Soc. Rev.* **2009**, *38*, 2520−2531.

(3) Simon, P.; Gogotsi, Y. Materials for electrochemical capacitors. Electrochemical Capacitors for Energy Management. *Nat. Mater.* **2008**, *7*, 845−854.

(4) Fic, K.; Meller, M.; Frackowiak, E. Strategies for Enhancing the Performance of Carbon/Carbon Supercapacitors in Aqueous Electrolytes. *Electrochim. Acta* **2014**, *128*, 210−217.

(5) Zhai, Y.; Dou, Y.; Zhao, D.; Fulvio, P. F.; Mayes, R. T.; Dai, S. Carbon Materials for Chemical Capacitive Energy Storage. *Adv. Mater.* **2011**, *23*, 4828−4850.

(6) Inagaki, M.; Konno, H.; Tanaike, O. Carbon Materials for Electrochemical Capacitors. *J. Power Sources* **2010**, *195*, 7880−7903.

(7) Frackowiak, E.; Béguin, F. Carbon Materials for the Electrochemical Storage of Energy in Capacitors. *Carbon* **2001**, *39*, 937−950.

(8) Nishihara, H.; Kyotani, T. Templated Nanocarbons for Energy Storage. *Adv. Mater.* **2012**, *24*, 4473−4498.

(9) Xia, K.; Gao, Q.; Jiang, J.; Hu, J. Hierarchical Porous Carbons with Controlled Micropores and Mesopores for Supercapacitor Electrode Materials. *Carbon* **2008**, *46*, 1718−1726.

(10) Chmiola, J.; Yushin, G.; Gogotsi, Y.; Portet, C.; Simon, P.; Taberna, P. L. Anomalous Increase in Carbon Capacitance at Pore Sizes Less Than 1 Nanometer. *Science* **2006**, *313*, 1760−1763.

(11) Huang, J.; Sumpter, B. G.; Meunier, V. Theoretical Model for Nanoporous Carbon Supercapacitors. *Angew. Chem., Int. Ed.* **2008**, *47*, 520−524.

(12) Yuan, C. Z.; Gao, B.; Shen, L. F.; Yang, D. S.; Hao, L.; Lu, X. J.; Zhang, F.; Zhang, L. J.; Zhang, X. G. Hierarchically Structured

Carbon-Based Composites: Design, Synthesis and Their Application in Electrochemical Capacitors. *Nanoscale* **2011**, *3*, 529−545.
(13) Ania, C. O.; Khomenko, V.; Raymund-Piñero, E.; Parra, J. B.; Béguin, F. The Large Electrochemical Capacitance of Microporous Doped Carbon Obtained by Using a Zeolite Template. *Angew. Chem., Int. Ed.* **2007**, *17*, 1828−1836.
(14) Hall, P. J.; Mirzaeian, M.; Fletcher, S. I.; Sillars, F. B.; Rennie, A. J. R.; Shitta-Bey, G. O.; Wilson, G.; Cruden, A.; Carter, R. Energy Storage in Electrochemical Capacitors: Designing Functional Materials to Improve Performance. *Energy Environ. Sci.* **2010**, *3*, 1238−1251.
(15) Hulicova-Jurcakova, D.; Puziy, A. M.; Poddubnaya, O. I.; Suárez-García, F.; Tascón, J. M. D.; Lu, G. Q. Highly Stable Performance of Supercapacitors from Phosphorus-Enriched Carbons. *J. Am. Chem. Soc.* **2009**, *131*, 5026−5027.
(16) Kim, C.; Ngoc, B. T. N.; Yang, K. S.; Kojima, M.; Kim, Y. A.; Kim, Y. J.; Endo, M.; Yang, S. C. Self-Sustained Thin Webs Consisting of Porous Carbon Nanofibers for Supercapacitors via the Electrospinning of Polyacrylonitrile Solutions Containing Zinc Chloride. *Adv. Mater.* **2007**, *19*, 2341−2346.
(17) Yan, J.; Wei, T.; Qiao, W.; Fan, Z.; Zhang, L.; Li, T.; Zhao, Q. A High-Performance Carbon Derived from Polyaniline for Supercapacitors. *Electrochem. Commun.* **2010**, *12*, 1279−1282.
(18) Xu, B.; Hou, S.; Cao, G.; Wu, F.; Yang, Y. S. Sustainable Nitrogen-Doped Porous Carbon with High Surface Areas Prepared from Gelatin for Supercapacitors. *J. Mater. Chem.* **2012**, *22*, 19088−19093.
(19) Hong, X.; Hui, K. S.; Zeng, Z.; Hui, K. N.; Zhang, L.; Mo, M.; Li, M. Hierarchical Nitrogen-Doped Porous Carbon with High Surface area Derived from Endothelium Corneum Gigeriae Galli for High-Performance Supercapacitor. *Electrochim. Acta* **2014**, *130*, 464−469.
(20) Yagci, Y.; Kiskan, B.; Ghosh, N. N. Recent Advancement on Polybenzoxazine—A Newly Developed High Performance Thermoset. *J. Polym. Sci., Part A: Polym. Chem.* **2009**, *47*, 5565−5576.
(21) Ghosh, N. N.; Kiskan, B.; Yagci, Y. Polybenzoxazines—New High Performance Thermosetting Resins: Synthesis and Properties. *Prog. Polym. Sci.* **2007**, *32*, 1344−1391.
(22) Liu, X.; Gu, Y. Study on the Volumetric Expansion of Benzoxazine Curing with Different Catalysts. *J. Appl. Polym. Sci.* **2002**, *84*, 1107−1113.
(23) Agag, T.; Arza, C. R.; Maurer, F. H. J.; Ishida, H. Primary Amine-Functional Benzoxazine Monomers and Their Use for Amide-Containing Monomeric Benzoxazines. *Macromolecules* **2010**, *43*, 2748−2758.
(24) Sawaryn, C.; Landfester, K.; Taden, A. Benzoxazine Miniemulsions Stabilized with Polymerizable Nonionic Benzoxazine Surfactants. *Macromolecules* **2010**, *43*, 8933−8941.
(25) Sawaryn, C.; Landfester, K.; Taden, A. Benzoxazine Miniemulsions Stabilized with Multifunctional Main-chain Benzoxazine Protective Colloids. *Macromolecules* **2011**, *44*, 5650−5658.
(26) Hao, G. P.; Li, W. C.; Qian, D.; Wang, G. H.; Zhang, W. P.; Zhang, T.; Wang, A. Q.; Schüth, F.; Bongard, H. J.; Lu, A. H. Structurally Designed Synthesis of Mechanically Stable Poly(Benzoxazine-*co*-Resol)-Based Porous Carbon Monoliths and Their Application as High-Performance CO_2 Capture Sorbents. *J. Am. Chem. Soc.* **2011**,, *133*,, 11378-−11388..
(27) Cao, G. P.; Chen, W. J.; Liu, X. B. Synthesis and Thermal Properties of the Thermosetting Resin based on Cyano Functionalized Benzoxazine. *Polym. Degrad. Stab.* **2008**, *93*, 739−744.
(28) Meng, Y.; Gu, D.; Zhang, F.; Shi, Y.; Yang, H.; Li, Z.; Yu, C.; Tu, B.; Zhao, D. Ordered Mesoporous Polymers and Homologous Carbon Frameworks: Amphiphilic Surfactant Templating and Direct Transformation. *Angew. Chem.* **2005**, *117*, 7215−7221.
(29) Baqar, M.; Agag, T.; Huang, R.; Maia, J.; Qutubuddin, S.; Ishida, H. Mechanistic Pathways for the Polymerization of Methylol-Functional Benzoxazine Monomers. *Macromolecules* **2012**, *45*, 8119−8125.
(30) Brunovska, Z.; Lvon, R.; Ishida, H. Thermal Properties of Phthalonitrile Functional Polybenzoxazines. *Thermochim. Acta* **2000**, *357*−*358*, 195−203.
(31) Zhao, Q.; Wang, X.; Wu, C.; Liu, J.; Wang, H.; Gao, J.; Zhang, Y. Supercapacitive Performance of Hierarchical Porous Carbon Microspheres Prepared by Simple One-Pot Method. *J. Power Sources* **2014**, *254*, 10−17.
(32) Jin, H.; Wang, X.; Gu, Z.; Polin, J. Carbon Materials from High Ash Biochar for Supercapacitor and Improvement of Capacitance with HNO_3 Surface Oxidation. *J. Power Sources* **2013**, *236*, 285−292.
(33) Yuan, D.; Chen, J.; Zeng, J.; Tan, S. Preparation of Monodisperse Carbon Nanospheres for Electrochemical Capacitors. *Electrochem. Commun.* **2008**, *10*, 1067−1070.
(34) Wang, Q.; Yan, J.; Wang, Y.; Ning, G.; Fan, Z.; Wei, T.; Cheng, J.; Zhang, M.; Jing, X. Template Synthesis of Hollow Carbon Spheres Anchored on Carbon Nanotubes for High Rate Performance Supercapacitors. *Carbon* **2013**, *52*, 209−218.
(35) Hulicova-Jurcakova, D.; Kodama, M.; Shirashi, S.; Hatori, H.; Zhu, Z. H.; Lu, G. Q. Nitrogen-Enriched Nonporous Carbon Electrodes with Extraordinary Supercapacitance. *Adv. Funct. Mater.* **2009**, *19*, 1800−1809.
(36) Wu, J.; Zhang, D.; Wang, Y.; Hou, B. R. Electrocatalytic Activity of Nitrogen-Doped Graphene Synthesized via a One-Pot Hydrothermal Process Towards Oxygen Reduction Reaction. *J. Power Sources* **2013**, *227*, 185−190.
(37) Andreas, H. A.; Conway, B. E. Examination of the Double-Layer Capacitance of an High Specific-Area C-Cloth Electrode as Titrated from Acidic to Alkaline pHs. *Electrochim. Acta* **2006**, *51*, 6510−6520.
(38) Kerisit, S.; Schwenzer, B.; Vijayakumar, M. Effects of Oxygen-Containing Functional Groups on Supercapacitor Performance. *J. Phys. Chem. Lett.* **2014**, *5*, 2330−2334.
(39) Fujisawa, K.; Cruz-Silva, R.; Yang, K. S.; Kim, Y. A.; Hayashi, T.; Endo, M.; Terrones, M.; Dresselhaus, M. S. Importance of Open, Heteroatom-Decorated Edges in Chemically Doped-Graphene for Supercapacitor Applications. *J. Mater. Chem. A* **2014**, *2*, 9532−9540.
(40) Wickramaratne, N. P.; Xu, J.; Wang, M.; Zhu, L.; Dai, L.; Jaroniec, M. Nitrogen Enriched Porous Carbon Spheres: Attractive Materials for Supercapacitor Electrodes and CO_2 Adsorption. *Chem. Mater.* **2014**, *26*, 2820−2828.
(41) Candelaria, S. L.; Garcia, B. B.; Liu, D.; Cao, G. Nitrogen Modification of Highly Porous Carbon for Improved Supercapacitor Performance. *J. Mater. Chem.* **2012**, *22*, 9884−9889.
(42) Lee, Y. H.; Chang, K. H.; Hu, C. C. Differentiate the Pseudocapacitance and Double-Layer Capacitance Contributions for Nitrogen-Doped Reduced Graphene Oxide in Acidic and Alkaline Electrolytes. *J. Power Sources* **2013**, *227*, 300−308.
(43) Guo, Y.; Shi, Z.; Chen, M. M.; Wang, C. Y. Hierarchical Porous Carbon Derived from Sulfonated Pitch for Electrical Double Layer Capacitors. *J. Power Sources* **2014**, *252*, 235−43.
(44) Yang, X.; Wu, D.; Chen, X.; Fu, R. Nitrogen-Enriched Nanocarbons with a 3-D Continuous Mesopore Structure from Polyacrylonitrile for Supercapacitor Application. *J. Phys. Chem. C* **2010**, *114*, 8581−8586.
(45) Wang, D. W.; Li, F.; Chen, Z. G.; Gao, Q. L.; Cheng, H. M. Synthesis and Electrochemical Property of Boron-Doped Mesoporous Carbon in Supercapacitor. *Chem. Mater.* **2008**, *20*, 7195−7200.
(46) Chmiola, J.; Yushin, G.; Dash, R.; Gogotsi, Y. Effect of Pore Size and Surface Area of Carbide Derived Carbons on Specific Capacitance. *J. Power Sources* **2006**, *158*, 765−772.
(47) Yu, P.; Li, Y.; Zhao, X.; Wu, L.; Zhang, Q. Graphene-Wrapped Polyaniline Nanowire Arrays on Nitrogen-Doped Carbon Fabric as Novel Flexible Hybrid Electrode Materials for High-Performance Supercapacitor. *Langmuir* **2014**, *30*, 5306−5313.
(48) Nasini, U. B.; Bairi, V. G.; Ramasahayam, S. K.; Bourdo, S. E.; Viswanathan, T.; Shaikh, A. U. Phosphorous and Nitrogen Dual Heteroatom Doped Mesoporous Carbon Synthesized via Microwave Method for Supercapacitor Application. *J. Power Sources* **2014**, *250*, 257−265.
(49) Xu, B.; Hou, S. S.; Zhang, F. L.; Cao, G. P.; Chu, M.; Yang, Y. S. Nitrogen-Doped Mesoporous Carbon Derived from Biopolymer as Electrode Material for Supercapacitors. *J. Electroanal. Chem.* **2014**, *712*, 146−150.

(50) Yuan, D.; Zhou, T.; Zhou, S.; Zou, W.; Mo, S.; Xia, N. Nitrogen-Enriched Carbon Nanowires from the Direct Carbonization of Polyaniline Nanowires and its Electrochemical Properties. *Electrochem. Commun.* **2011**, *13*, 242−246.
(51) Zhao, L.; Fan, L. Z.; Zhou, M. Q.; Guan, H.; Qiao, S.; Antonietti, M.; Titirici, M. M. Nitrogen-Containing Hydrothermal Carbons with Superior Performance in Supercapacitors. *Adv. Mater.* **2010**, *22*, 5202−5206.
(52) Wei, J.; Zhou, D.; Sun, Z.; Deng, Y.; Xia, Y.; Zhao, D. A Controllable Synthesis of Rich Nitrogen-Doped Ordered Mesoporous Carbon for CO_2 Capture and Supercapacitors. *Adv. Funct. Mater.* **2013**, *23*, 2322−2328.
(53) Chen, X. Y.; Chen, C.; Zhang, Z. J.; Xie, D. H.; Deng, X.; Liu, J. W. Nitrogen-Doped Porous Carbon for Supercapacitor with Long-Term Electrochemical Stability. *J. Power Sources* **2013**, *230*, 50−58.
(54) Frackowiak, E. Carbon Materials for Supercapacitor Application. *Phys. Chem. Chem. Phys.* **2007**, *9*, 1774−1785.
(55) Chen, L. F.; Zhang, X. D.; Liang, H. W.; Kong, M. G.; Guan, Q. F.; Chen, P.; Wu, Z. Y.; Yu, S. H. Synthesis of Nitrogen-Doped Porous Carbon Nanofibers as an Efficient Electrode Material for Supercapacitors. *ACS Nano* **2012**, *6*, 7092−7102.